Environmental Earth Sciences (2021) 80:247
https://doi.org/10.1007/s12665-021-09556-z

ORIGINAL ARTICLE

Estimation and validation of groundwater vulnerability of an urban aquifer using GIS and DRASTIC: City of Monterrey, Mexico

Héctor de León-Gómez[1] · Miguel A. Martin del Campo-Delgado[1] · María V. Esteller-Alberich[2] · Saraí García-González[1] · Arquímedes Cruz-López[1] · Héctor D. de León-Rodríguez[1] · Mariana Pérez-Martínez[1] · Víctor H. Guerra-Cobián[1]

Received: 2 October 2020 / Accepted: 8 March 2021 / Published online: 18 March 2021

Abstract
The Monterrey wellfield is located in the urban aquifer of the Monterrey Metropolitan Area (Mexico), and has been subject to considerably increasing stress. This area is constantly growing, both in terms of infrastructure and population. The overall objective of the present study is to assess and validate the aquifer's vulnerability to contamination by applying hydrogeological and hydrogeochemical methods. To this end, four campaigns to measure depth of groundwater were conducted and three water sampling surveys were carried out during in 2018 and 2019, when drought conditions existed. The hydrogeological results show that the groundwater mainly flows from southwest to northeast direction. With regard to hydrogeochemical findings, the type of water was determined by Ca^{2+}, Na^{+}, Mg^{2+}, Cl^{-} ions, which can be altered by SO_4^{2-} concentrations. A vulnerability map was also constructed using the DRASTIC method, which indicates that the most vulnerable areas were contaminated by anthropogenic influences, where SO_4^{2-}, Cl^{-}, Fe, Al, and coliforms were present.

Keywords Hydrogeology · Hydrogeochemistry · Porous aquifer · Vulnerability · Pollution

Introduction

Groundwater is a valuable natural resource that has been used to supply populations, agricultural activities, as well as industrial and recreational activities. This resource is stored in geological formations called aquifers (Custodio and Llamas 1983). These geological formations can be classified into hydrogeological units, based on the lithological characteristics and according to the hydrostatic pressure (Diaz-Delgado et al. 2006). However, at present, we cannot ignore the relationship between groundwater flow systems and the different elements that make up cities, such as infrastructure, economic activities, and the demand of the population to satisfy their needs, as well as the environmental impact of pollution that is generated derived from the inappropriate disposal of its waste. For this reason, urban hydrogeology arises, and with it, the term "urban aquifer", as a necessity to understand and explain the processes of chemical and hydrodynamic interaction between subterranean water resources and the urban environment (Schirmer et al. 2013).

It is important to consider many factors have considerably increased stress on groundwater resources, especially in arid–semiarid regions where groundwater is the main source of water supply. Causes of stress are population growth, agricultural and industrial activities, poor management of aquifers, and the current impact of climate change (Neshat et al. 2014; Martin del Campo et al. 2014; Srinivasamoorthy 2014; Kazakis and Voudouris 2015; Hassane et al. 2016; Oudraogo et al. 2016; MacDonald et al. 2016; Huang et al. 2018; Lapworth et al. 2018; Li et al. 2018a, b).

Another stress factor is the pollution process. Knowledge about hydrochemical characteristics helps to identify the relationship between geochemical processes and groundwater quality, and to determine whether a pollution problem associated with a factor other than geology exists, such as

✉ Héctor de León-Gómez
hector.deleongm@uanl.edu.mx

[1] Facultad de Ingeniería Civil, Universidad Autónoma de Nuevo León (UANL), Av. Universidad S/N, Cd. Universitaria, 66455 San Nicolás de los Garza, Nuevo León, México

[2] Instituto Interamericano de Tecnología Y Ciencias del Agua (IITCA), Universidad Autónoma del Estado de México (UAEM), Carretera Toluca-Ixtlahuaca km. 14.5 San Cayetano Morelos, 50120 Toluca, México

agricultural, urban, or industrial activities (Dragon & Gorski 2015; Chenini et al. 2015; Shrestha et al. 2016; Lapworth et al. 2018; AlSuhaimi et al. 2017; Samantra et al. 2017; Li et al. 2018a, b).

Urban aquifers are very likely to be affected by polluting activities. Various studies have been carried out to identify the quality of the groundwater in urban aquifers, and most of them agree that infiltration of wastewater is the main source of contamination for these types of aquifers. This type of contamination is reflected by high concentrations of nitrates, as indicated by Waguespack (2019), Zendehbad et al. (2019), Daneshian et al. (2020) and da Silva Peixoto et al. (2020).

The term "vulnerability" is used to describe the sensitivity of an aquifer system to polluting activities (Valcarce & Jiménez 2016). Vulnerability maps are a very useful tool for representing priority areas for groundwater protection and for determining the degree to which groundwater is vulnerable to pollution (Nanou et al. 2018).

Various authors have used different methods to determine the vulnerability of groundwater to pollution (Pórcel et al. 2014; Shrestha et al. 2016; Paredes et al. 2018). One of these methods include the variables of depth of groundwater (*D*), net recharge (*R*), aquifer media (*A*), soil media (*S*), topography (*T*), impact of the vadose zone (*I*), and hydraulic conductivity (*C*), and is better known as DRASTIC, that is one of the most used and helpful methods (Machiwal et al. 2018). However, while identifying groundwater vulnerability is important for managing water resources, it is dependent on the availability of data and the complexity of hydrogeological conditions (Garfias et al. 2017).

The methods used to assess the vulnerability of aquifers are generally modified to integrate other important parameters or variables or combined and supported with other methods or models to identify the areas where contamination is most likely to occur and obtain more precisely results from vulnerability maps, as did Neshat et al. (2014) and Kazakis & Voudouris, (2015). They used as support resources the Analytical Hierarchy Process (AHP), the Wilcoxon rank-sum nonparametric statistical test (Neshat et al. 2014), the Effects of Groundwater Loading of Agricultural Management Systems (GLEAMS) and the Analysis of Variance (ANOVA) (Kazakis and Voudouris 2015).

Shrestha et al. (2016) used DRASTIC along with the Groundwater Risk Assessment Model (GRAM) to assess vulnerability and the risk of groundwater contamination for different rainfall regimes. Their vulnerability and risk maps informed planning and groundwater protection policies.

Garfias et al. (2017) performed a study to evaluate the vulnerability of the Toluca Valley aquifer, Mexico, using DRASTIC and the numerical modeling of groundwater flow with particle tracking (advective transport). Those results made it possible to identify and consider all the factors and sites that were susceptible to contamination, not only those shown on the vulnerability map.

In the city of Mashhad, Iran, Asadi et al. (2017) evaluated the vulnerability of an aquifer to anthropogenic activities, given that the groundwater in that aquifer was being contaminated by domestic wastewater.

It is also important to consider that urban aquifers are subject to high rates of groundwater extraction, which can cause subsidence, cracking, and damage to urban infrastructure, increasing the risk of pollutant propagation and infiltration, as Hernández-Espriú et al. (2014) and Paredes et al. (2018) pointed.

The main objective of the present work based on GIS-based mapping and the DRASTIC vulnerability method to assess and validate the degree to which groundwater in an urban aquifer was vulnerable to contamination. The integrated use of these techniques with the hydrodynamic and hydrochemical behavior of the study area produced new information about aquifer vulnerability and its validation. The vulnerability map generated by this study is useful for groundwater management and urban planning in the study area.

Description of the study area

The Monterrey wellfield is located in the Monterrey Valley, which encompasses the cities of Monterrey, San Nicolás de los Garza, Guadalupe, San Pedro Garza García, and Santa Catarina (Fig. 1). The population was 2,642,304 inhabitants in the last census, in 2015 (INEGI 2020). Land use in the valley is mainly residential–urban–industrial, where economic activities by the tertiary sector are predominant (Gobierno del Estado de Nuevo Leon 2016).

The Monterrey Valley in northern Mexico and is part of three physiographic provinces in the country: Sierra Madre Oriental (SMO), Northern Gulf Coastal Plains (NGCP), and the Great Plains of North America (GPNA) (INEGI 2008). This is a semiarid region with a variety of climates, although extreme dry and semi-dry climates predominate, making the region highly vulnerable to water scarcity (Ortega and Velasco 2013). The annual average temperature is 22 °C and annual average precipitation is roughly 600 mm (CONAGUA 2019).

The main geological in this region is Quaternary fluvial sediment deposits consisting of gravel, silt, clay, and sand (Alva Niño 1997), with a few shale outcrops of the Upper Cretaceous Mendez Formation (Campanian–Maastrichtian).

The Monterrey wellfield draws water from a semiconfined urban aquifer. This aquifer is mainly of gravel packed in silty clay, gravel, and partially cemented conglomerates. The bottom of the aquifer is impermeable and is made of fractured Mendez shale (Hernández 1999). It has an average hydraulic

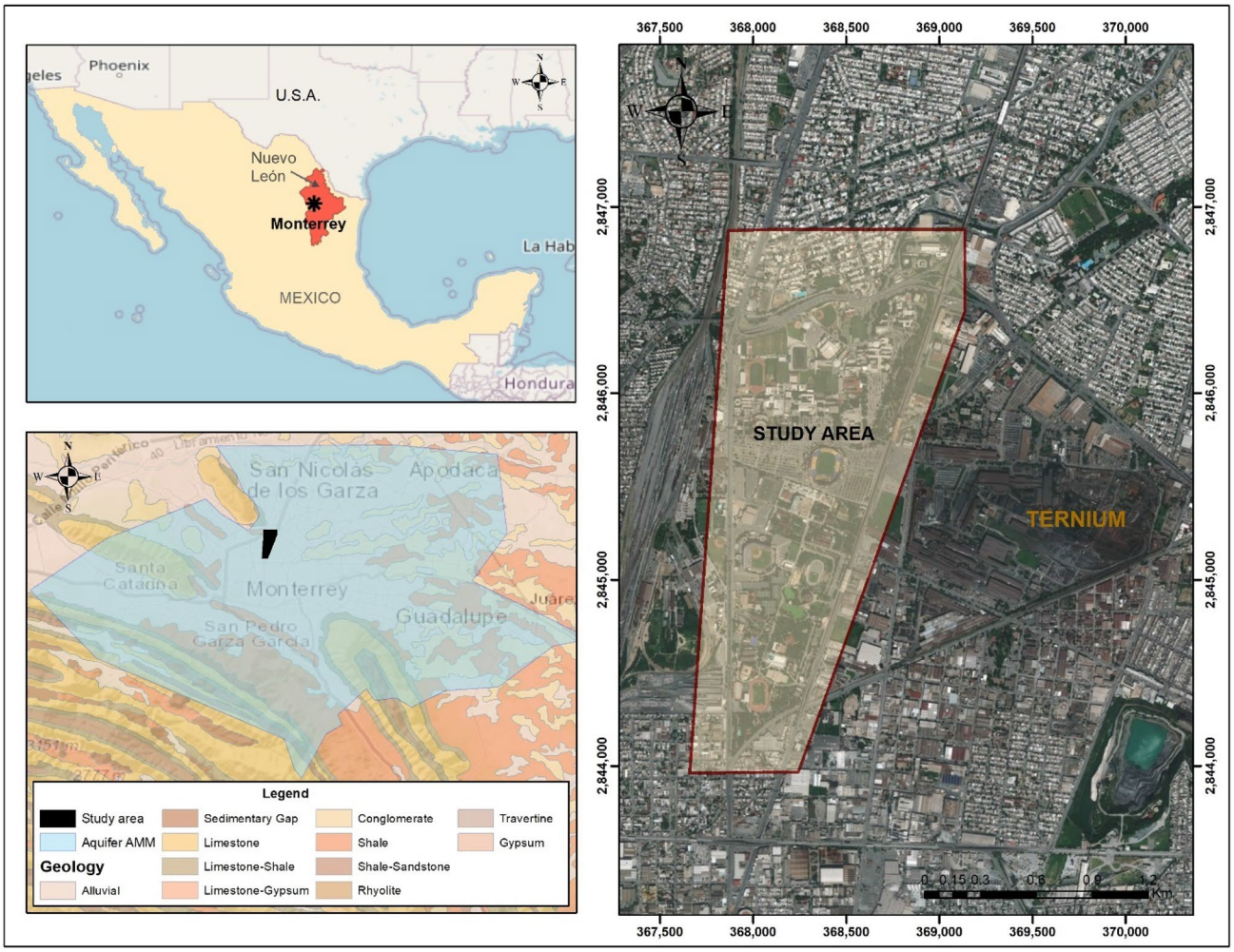

Fig. 1 Study area location: **a** Nuevo Leon State, **b** aquifer of the Monterrey Metropolitan Area, **c** study area (modified from Google, 2019)

conductivity of 92 m/day and a total average extraction volume of 3 m^3/s (Monterrey Water and Drainage Services, Servicios de Agua y Drenaje de Monterrey—SayDM, in Spanish, 2018).

A 3-km^2 urban industrial portion of the Monterrey wellfield was selected as the study area (Fig. 1). Ten wells used for public urban supply have been identified in the study area (Fig. 2). Their average depth is 60 m and they are in constant operation. It is important to note that the groundwater level ranges from 11 to 18 m deep and the groundwater mainly flows from southwest to northeast (Silva et al. 2015).

Problems with insufficient water supply from long periods of drought in the region have been identified, as has an increase in the volume of water extracted to satisfy human consumption. For this reason, water storage tanks have been installed to cover basic water needs (Hernández 1999). It is worth mentioning that garden irrigation has been carried out since 2018 (the study area includes university infrastructure such as gardens and sports fields) with treated wastewater supplied by the Monterrey Water and Drainage Services (Servicios de Agua y Drenaje de Monterrey—SAyDM, in Spanish), and this water usually has high values of TDS, SO_4^{2-}, Cl^-, NO_3^-, and coliforms.

It is also important to note that TERNIUM, a leading company in the steel industry, is located to the east of the study area. Their activities range from extracting iron ore from their own mines to manufacturing steel and products. Negative effects on the environment can be seen on the ground surface, where the surrounding terrain has a gray tone, and the urban infrastructure has been affected by corrosion.

For these reasons, this study area was selected to monitor the hydrodynamic and hydrogeochemistry of the groundwater, as well as to determine the degree to which groundwater has been affected and implications for environmental problems.

Materials and methods

This work used hydrodynamic and hydrogeochemical and microbiological information along with the DRASTIC vulnerability method (Aller et al. 1987) to assess groundwater vulnerability. And Fig. 2 explains the main steps along the investigation.

Hydrodynamic

The evolution of groundwater table levels over the period 2008–2015 was analyzed based on databases provided by Servicios de Agua y Drenaje de Monterrey (SAyDM) (Table 1). However, these databases only contained five of the wells that are located in the study area. Therefore, field visits were conducted between 2016 and 2019 to verify the location of the wells that were previously registered in the SAyDM databases, as well as to obtain additional points for measuring groundwater levels (Table 2, Fig. 3). A database was created based on the information from the SAyDM and the field visits, which was later exported to a Geographic Information System (GIS) in ArcGIS 10.3. The location of sampling wells were recorded in the projected coordinate system WGS 1984, UTM Zone: 14 N.

Groundwater table levels were processed in ArcGIS 10.3 using the Kriging mathematical method and the hydrological triangle.

Physicochemical and microbiological analyses

Three sampling campaigns were carried out: the first in June 2018, the second in February 2019, and the third in May 2019. All procedures and sample collections were performed according to Mexican standard NOM-230-SSA1-2002, which establishes the sanitary procedures for sampling water for human use and consumption. Physical parameters such as pH, electrical conductivity, and temperature were measured in situ using an Orion 5-Star Plus multiparameter. Plastic containers and lids were used for the anion analysis. For the analysis of cations and heavy metals, 1 mL of concentrated nitric acid (0.015 N) was added per 100 mL of filtered water sample to obtain a $pH \leq 2$.

The samples collected were sent to certified laboratories. For the physicochemical and bacteriological analyses, the samples were sent to the Professional Services Laboratory of the School of Chemical Sciences (Universidad Autónoma de Nuevo León, UANL in Spanish). These analyses were performed in accordance with Mexican regulations (Table 3). The microbiological analysis (fecal and total coliform) was conducted using glass bottles with a ground-glass stopper, sterile disposable bottles, or sterile bags with a tight seal and a capacity of 125 or 150 mL. Heavy metals were analyzed at the Actlabs Laboratory (Ontario, Canada) using mass spectrometry with induction-coupled plasma (ICP-MS, Thermo X series II model).

An electroneutrality balance was applied to these data according to ranges established by Freeze and Cherry (1979), which was useful for validating the results of the analyses. Piper diagrams were also constructed to obtain the hydrochemical characterization of the groundwater and to identify the predominant water facies.

Groundwater quality was evaluated based on Mexican standard NOM-127-SSA1-1994 "Environmental health and water for human use and consumption. Permissible quality

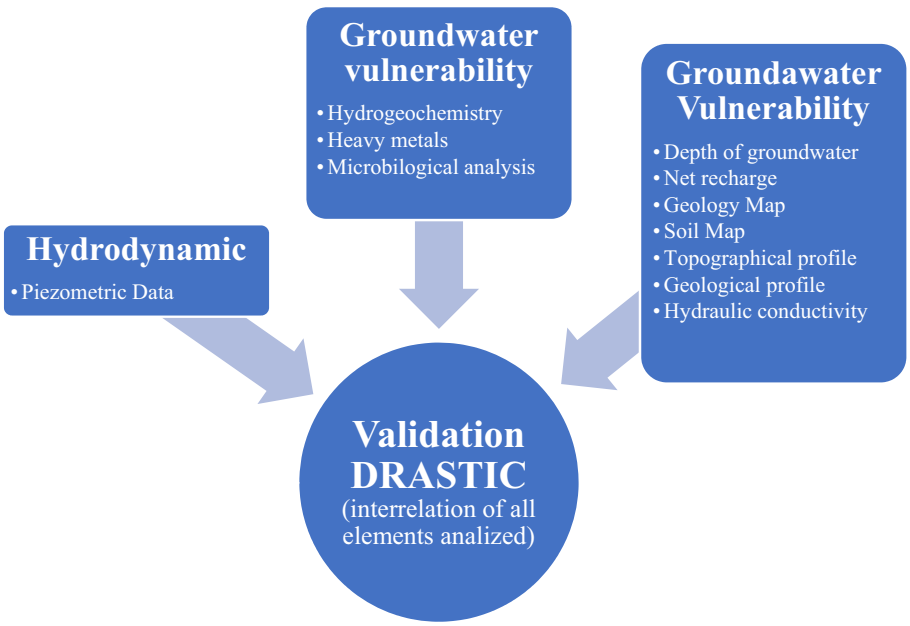

Fig. 2 Methodological scheme of the research work

Table 1 Study wells and depth of groundwater, 2008–2015 (SAyDM 2016)

Id (well)	Location (UTM) East	Location (UTM) North	Topographic elevation (m.a.s.l)	Depth (m)	Depth (m)	Depth (m)	Depth (m)	Depth (m)	Depth (m)	Depth (m)	Depth (m)
				2008	2009	2010	2011	2012	2013	2014	2015
PCU-4	368,752	2,845,963	517.50	10.65	11.50	12.23	12.48	12.76	12.46	12.78	12.42
PCU-6	367,918	2,845,652	523.80	N.D	N.D	N.D	12.12	13.09	12.40	12.38	12.20
PCU-8	367,989	2,845,486	525.00	14.42	14.67	14.61	14.03	14.03	13.75	13.66	14.09
PCU-9	368,152	2,844,143	530.50	12.59	14.75	13.11	10.97	10.93	11.40	11.40	11.28
PCU-10	368,724	2,845,876	518.00	11.29	12.28	12.34	13.36	13.03	12.42	12.50	12.21

m.a.s.l. meters above sea level, *ND* no data

limits and treatments to which water must be submitted for its purification."

Groundwater vulnerability

The DRASTIC vulnerability method is one of the most widely used methods, since it is very easy to apply in areas with insufficient data and it enables systematically evaluating study parameters. It includes seven parameters: depth of groundwater (D), net recharge (R), aquifer media (A), soil media (S), topography (T), impact vadose zone (I), and hydraulic conductivity (C). Table 4 presents the source of information for each of the parameters and the type of map (layer) obtained.

The vulnerability analysis involved categorizing each of the parameters mentioned into classes on a scale of 1–10, in which one denotes less vulnerable and ten most vulnerable areas. Weights were then assigned on a scale of 1–5, where one is less significant and five is more significant, according to the parameter's importance for determining the characteristics of the aquifer.

The DRASTIC vulnerability index (DVI) was calculated with the formula:

$$D_rD_w + R_rR_w + A_rA_w + S_rS_w + T_rT_w + I_rI_w + C_rC_w = \text{DVI} \quad (1)$$

where D_r = Rating for depth of groundwater, D_w = Weight assigned to the depth of groundwater, R_r = Rating for aquifer recharge, R_w = Weight for aquifer recharge, A_r = Rating assigned to aquifer media, A_w = Weight assigned to aquifer media, S_r = Rating for the soil media, S_w = Weight for the soil media, T_r = Rating for topography (slope), T_w = Weight assigned to topography, I_r = Rating assigned to impact of vadose zone, I_w = Weight assigned to impact of vadose zone, C_r = Rating for hydraulic conductivity rates, C_w = Weight given to hydraulic conductivity.

The vulnerability map of the study area was obtained by applying Eq. 1 with the Raster Calculator tool in ArcGIS 10.3 (Hussain et al. 2017; Lathamani et al. 2015; Shrestha et al. 2016). This was then reclassified according to the Jenks natural break statistical method, based on the Jenks break algorithm (the method proposed by the GIS used). The DVI was then divided into subclasses (high, medium, and low vulnerability) indicating the areas that are susceptible to groundwater contamination relative to other areas, where higher values correspond to greater vulnerability to groundwater contamination.

Table 2 Study wells and depth of groundwater, 2016–2019

Id (well)	Location (UTM) East	Location (UTM) North	Topographic elevation (m.a.s.l)	Depth (m) May 2016	Depth (m) July 2016	Depth (m) Feb. 2017	Depth (m) May 2017	Depth (m) May 2018	Depth (m) May 2019
PCU-1	368,883	2,846,757	514.00	15.00	14.93	14.82	14.98	14.93	15.00
PCU-2	368,820	2,846,726	514.50	16.42	16.07	15.85	16.06	16.07	16.27
PCU-3	368,986	2,846,607	513.50	15.64	15.53	15.37	15.52	15.53	15.57
PCU-4	368,752	2,845,963	517.50	12.97	12.92	12.73	12.88	12.41	12.46
PCU-5	368,006	2,844,904	527.00	12.05	11.89	11.58	11.74	13.93	14.96
PCU-6	367,918	2,845,652	523.80	12.55	12.36	12.34	12.42	12.20	12.18
PCU-7	368,557	2,845,420	521.00	14.90	14.71	14.52	14.76	12.01	11.79
PCU-8	367,989	2,845,486	525.00	14.45	14.29	13.98	14.14	14.40	14.17
PCU-9	368,152	2,844,143	530.50	11.68	11.52	11.21	11.38	11.40	11.42
PCU-10	368,724	2,845,876	518.00	12.93	12.77	12.46	12.62	12.63	12.66

m.a.s.l. meters above sea level

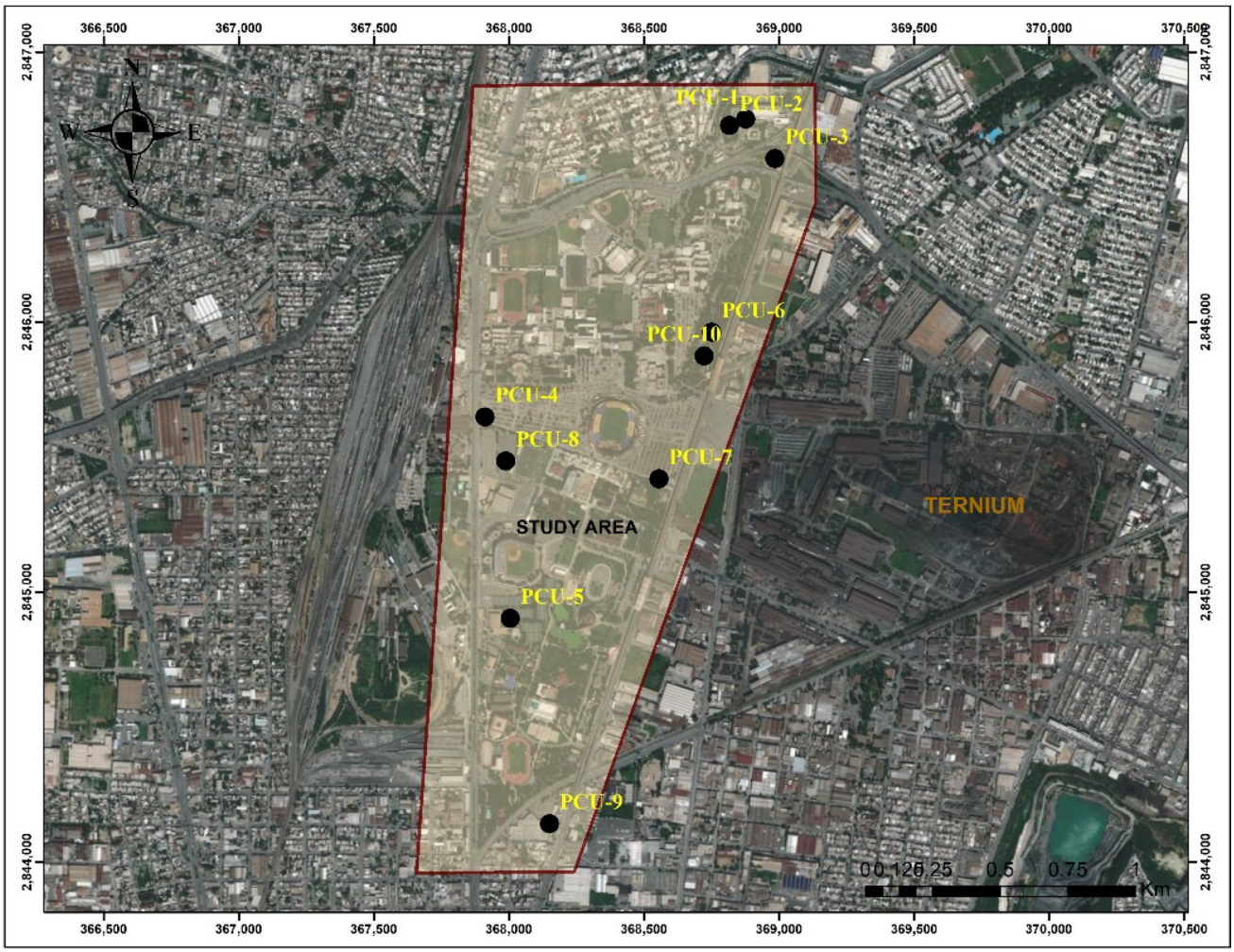

Fig. 3 Location of exploitation wells in the Monterrey wellfield study area

Table 3 Physicochemical and bacteriological analysis methods

Parameter	Method	Analysis method
Cl^- (mg/L)	Volumetric	NMX-AA-073-SCFI-2001
SO_4^2 (mg/L)	Turbidimetric	NMX-AA-074-1981
$N\text{-}NO_3^-$ (mg $N\text{-}NO_3$/L)	Volumetric	NMX-AA-079-SCFI-2001
HCO_3^- (mg HCO_3/L)	Volumetric	AWWA 2320
Total coliforms (MPN/100 mL)	Most Probable Number (MPN)	NOM-112-SSA1-1994
Fecal coliforms (MPN/100 mL)		NOM-145-SSA1-1995
Na^+ (mg/L)	Mass spectrometry with induction-coupled plasma	NMX-AA-051-SCFI-2001
K^+ (mg/L)		
Ca^{2+} (mg/L)		
Mg^{2+} (mg/L)		

Table 4 Data used for the DRASTIC method

Parameter	Map type	Source of information
D	Depth of groundwater	Monitoring of groundwater table levels
R	Net recharge	National Water Commission (CONAGUA 2019)
A	Geology map	Stratigraphic profiles by the Department of Soil Mechanics of the Institute of Civil Engineering, Autonomous University of Nuevo León (Hernández 1999; Silva et al. 2015)
S	Soil map	
T	Topographical sheet	Lidar (Laser Imaging Detection and Ranging) image with a resolution of 30 cm
I	Geological profile	Stratigraphic profiles by the Department of Soil Mechanics of the Institute of Civil Engineering, Autonomous University of Nuevo Leon (Hernández 1999; Silva et al. 2015)
C	Hydraulic conductivity	Hernández (1999) data

Results and discussion

Hydrodynamics

The 2008 map (Fig. 4a) shows groundwater levels ranging from 499 m.a.s.l in the far NE portion of the study area to 518 m.a.s.l in the far SW. The hydraulic gradient decreased in the direction of the groundwater flow (SW-NE). No significant changes in groundwater levels were found for the years 2009 and 2010. However, in 2011 (Fig. 4b), levels for wells PCU-6 and PCU-10 decreased notably more than the others due to groundwater exploitation to meet the university's needs. Meanwhile, no changes in groundwater levels were found in the study area in 2012, 2013, 2014, and 2015.

The most significant changes took place during the years 2016 and 2017 (Fig. 5a, b), when changes in groundwater flow occurred mainly due to exploitation, specifically in PCU-4, PCU-6, PCU-8, and PCU-10. It is important to mention that despite these changes, groundwater levels remained very similar to previous years.

While the groundwater table levels in 2018 and 2019 (Fig. 5c, d) were very similar to 2008, during other years, particularly 2016 and 2017, groundwater levels were primarily affected by two factors: transit time and the demand for groundwater. When demand is intense, it directly influences the dynamics of groundwater levels.

As can be seen in the groundwater level contour maps, the groundwater flows from southwest to northeast, and this direction did not change over the course of the years studied. This result is consistent with the flow direction shown by the groundwater table level maps in González (2011) and Navarro-Solís et al. (2016).

It is important to mention that the equidistance between the groundwater level curves is similar in the northeast and southwest portions of the study area, while it is greater in the central part where PCU-4, PCU-6, PCU-8, and PCU-10 are located. According to Darcy's Law, this would indicate differences in permeability. These results agree with Hernández (1999), who found that the aquifer had high hydraulic conductivity (K average = 92 m/day) and suitable characteristics for the extraction of groundwater.

As shown, groundwater levels generally remained constant from 2016 to 2019, reflecting the hydrodynamic conditions of a stable aquifer (Fig. 6). In this respect, a relationship can also be seen between precipitation and groundwater levels. As shown in Fig. 6, the groundwater depth was at its lowest in 2008 (12.25 m) and precipitation was 800 mm, while in 2009, precipitation did not exceed 500 mm and the

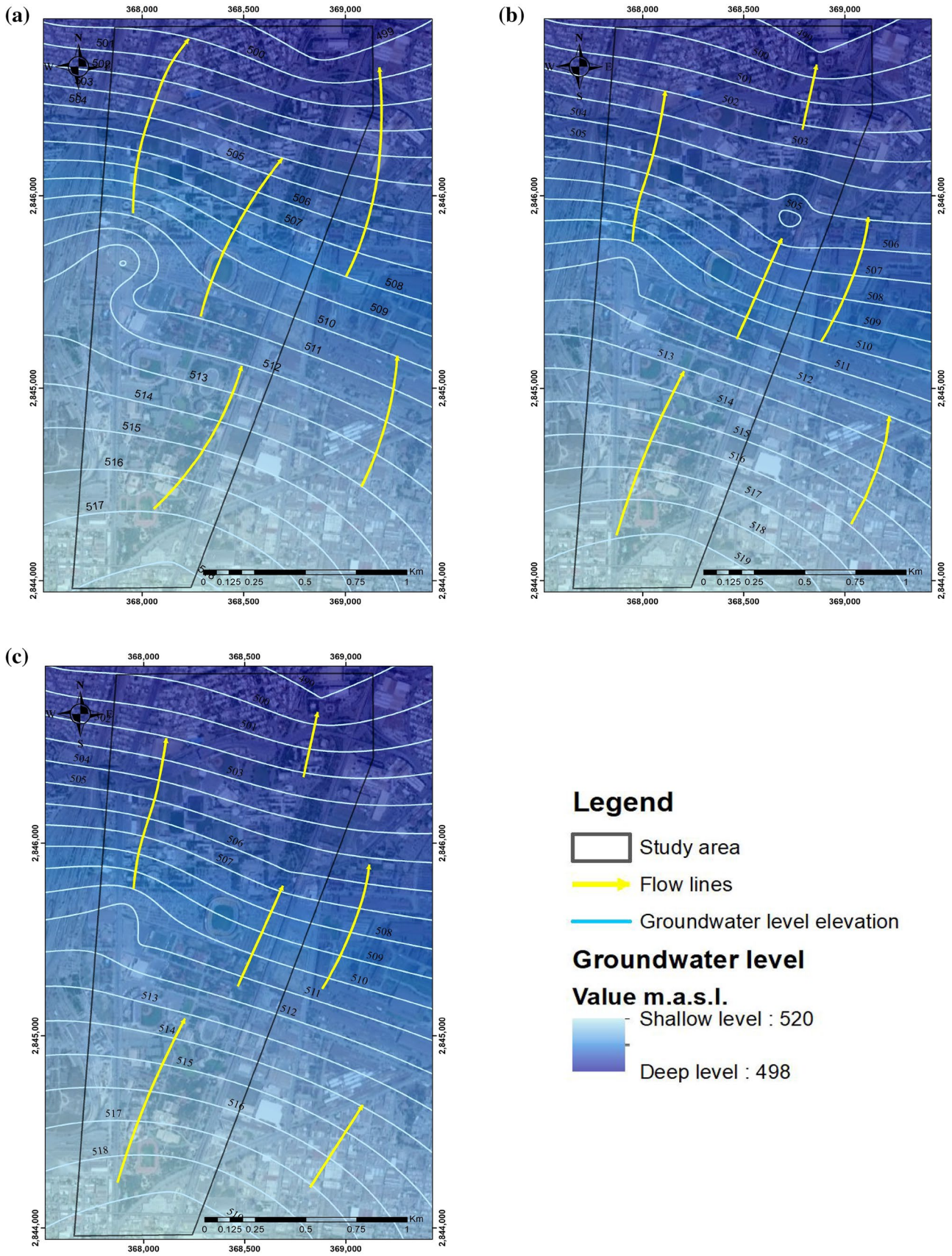

Fig. 4 Groundwater level contour map (meters above sea level) for: **a** 2008, **b** 2011, and **c** 2015

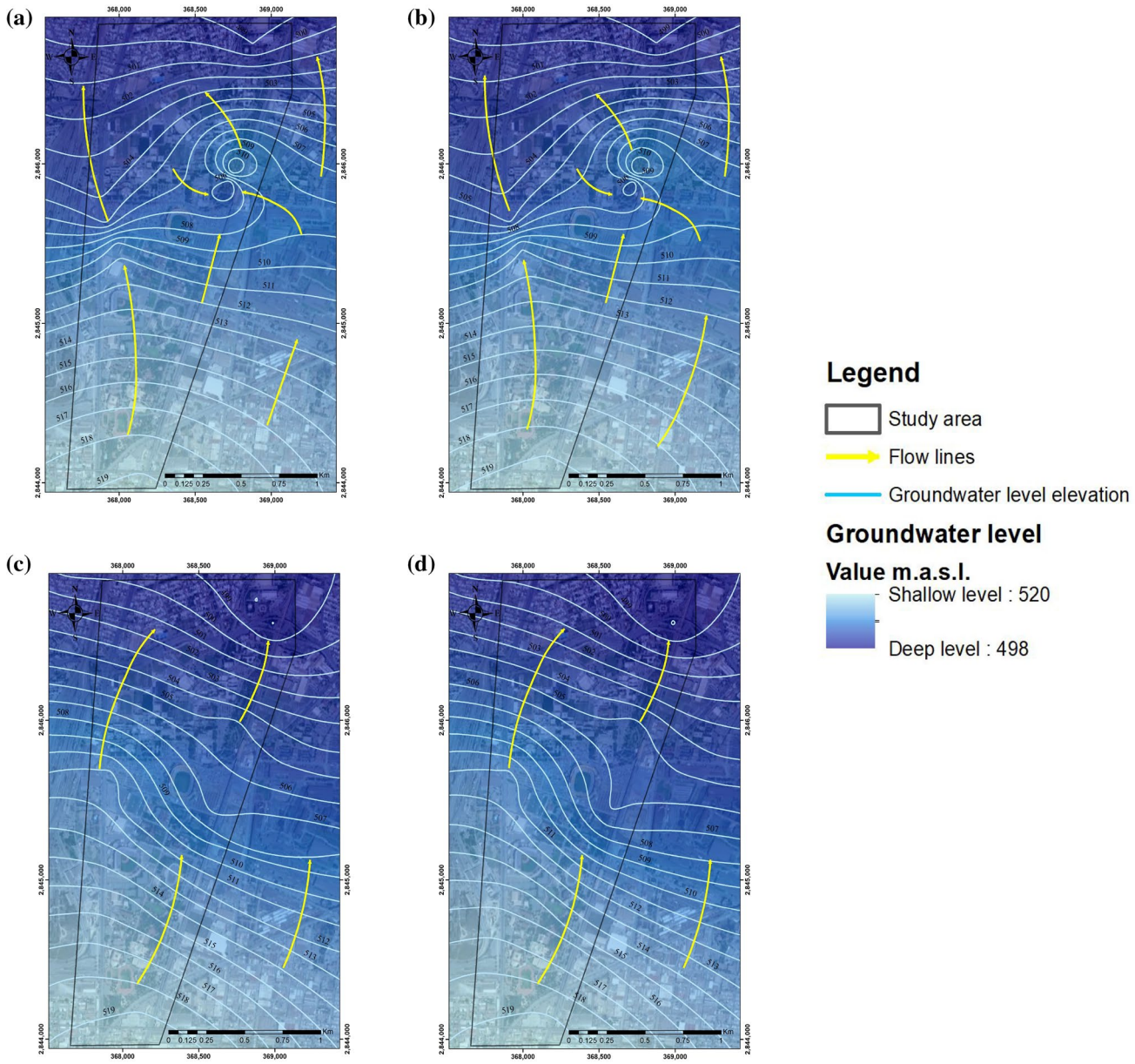

Fig. 5 Groundwater level contour map (meters above sea level): **a** 2016, **b** 2017, **c** 2018, and **d** 2019

groundwater level decreased one meter. During July 1 and 2, 2010, Hurricane Alex dropped nearly three times the normal annual precipitation for the City of Monterrey (of 600 mm) over 48 h, resulting in accumulated precipitation of approximately 1500 mm (Guerra-Cobian et al. 2015). However, this event was not considered to be important for the recharge of the aquifer. The lowest rainfall values were registered in 2011 and 2012, but they did not affect groundwater levels since those values (around 400 mm) did not have the same type of influence as in the year 2009. Groundwater levels recovered in 2013, 2014, and 2015 due to precipitation, and during the period 2016 to 2019, the depth of groundwater remained between 11 and 16 m (Fig. 6).

Hydrogeochemistry

Regarding in situ parameters (Table 5), no significant changes in temperature were found, with values ranging from 24.9 to 25.4 °C. The northeast portion of the study area had the highest temperature. The average pH value was 7.1. However, it is important to mention that the February 2019 sampling had the lowest pH, while no significant differences in pH were found between the June 2018 and May 2019 sampling (Table 5).

The average electrical conductivity was 1563 µS/cm. Wells PCU-1, PCU-2, and PCU-3, located in the northeastern portion of the study area, registered the highest electrical

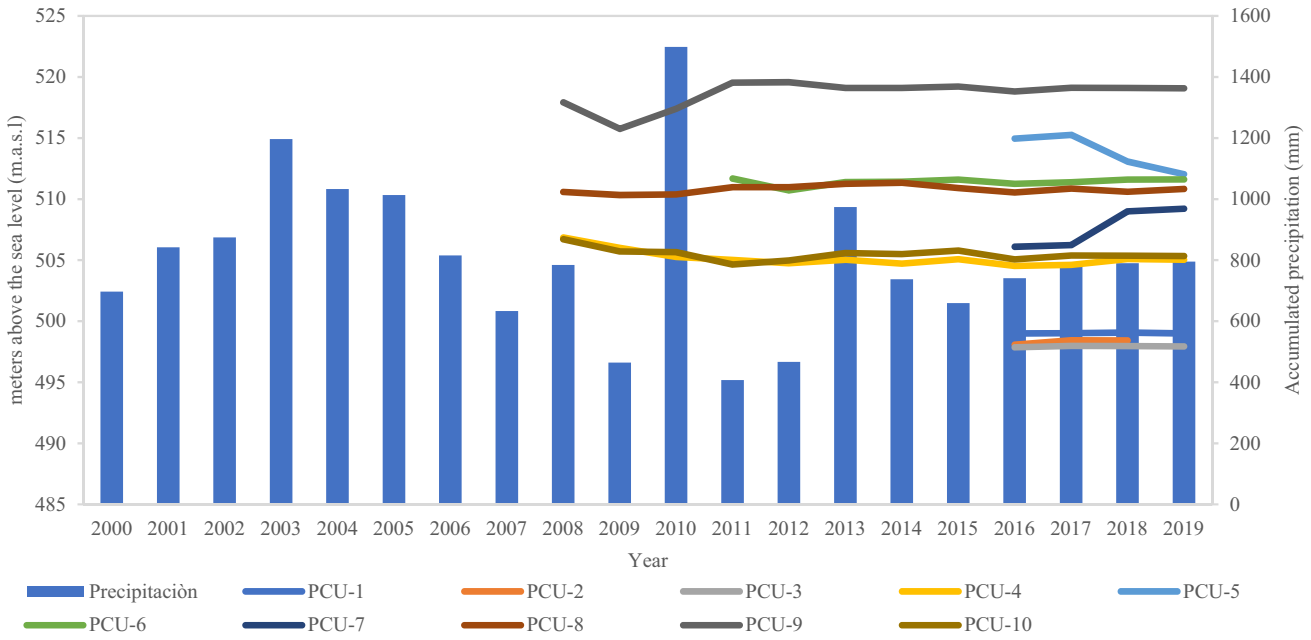

Fig. 6 Annual accumulated precipitation (2000–2019) at the City of Monterrey weather station (CONAGUA, 2019) and groundwater levels at the observation points

Table 5 Parameters measured in situ during sampling campaigns in June 2018, February 2019, and May 2019

	Temperature (°C)	pH	Electrical conductivity (µS/cm)
First sampling (June 2018)			
PCU-1	25.4	7.32	1683
PCU-2	25.0	7.28	1569
PCU-3	25.0	7.16	1238
PCU-4	25.3	7.20	902
PCU-5	25.0	7.40	788
PCU-6	25.1	7.16	987
PCU-7	25.1	7.20	819
Second sampling (February 2019)			
PCU-1	25.4	7.41	1515
PCU-2	25.4	6.91	1577
PCU-3	25.1	6.85	1136
PCU-4	25.3	6.86	883
PCU-5	25.2	7.30	796
PCU-6	25.1	6.87	983
PCU-7	24.9	6.91	785
Third sampling (May 2019))			
PCU-1	25.4	7.41	1917
PCU-2	25.4	7.01	1980
PCU-3	25.4	6.91	1430
PCU-4	25.1	6.85	1120
PCU-5	25.3	6.86	1020
PCU-6	25.1	6.87	1225
PCU-7	24.9	6.91	1260

conductivity values (Table 5). This may be due to the concentrations of dissolved anions and cations, which will be discussed in subsequent paragraphs.

Table 6 presents the chemical parameters of the groundwater samples. The electroneutrality balance (-5.9–5.8%) was within the range recommended by Freeze and Cherry (1979).

The concentration of Ca^{2+}, Mg^{2+}, Na^{+}, and K^{+} ions ranged from 120 to 219, 24 to 40, 24 to 169, and 1 to 5 mg/L, respectively (Table 6). The order of abundance was $Ca^{2+} > Na^{+} > Mg^{2+} > K^{+}$. With regard to anions, HCO_3^{-}, SO_4^{2-}, Cl^{-}, and NO_3^{-} ion concentrations ranged from 135 to 284, 90 to 462, 116 to 815, and 18 to 39 mg/L, respectively (Table 6). The order of their abundance was $Cl^{-}, > SO_4^{2-} > HCO_3^{-} > NO_3^{-}$. Wells PCU-1 and PCU-3 had high SO_4^{2-} and Cl^{-} contents.

A Piper diagram (Fig. 7) was constructed with data from the samples collected in 2018 and 2019 (Table 6). This shows the chemical facies of the groundwater, which are mixed waters and mainly calcium bicarbonate and calcium sulfate. The facies in the 2018 sampling were: 1) Ca-HCO_3 (PCU-2, PCU-4, PCU-6, and PCU-7), 2) Ca-SO_4 (PCU-3 and PCU-5), and 3) Ca–Cl (PCU-1). The water facies in the February 2019 samples were: 1) Ca-HCO_3 (PCU-1 and PCU-5) and 2) Ca-SO_4 (PCU-3, PCU-4, PCU-6 and PCU-7). The water facies in the May 2019 sampling were almost identical to those found in 2018, except for PCU-5 and PCU-7, which were Ca–SO_4 and Ca–HCO_3, respectively (Fig. 6, Table 6).

Table 6 Cation and anion concentrations (mg/L) for the samples collected during sampling campaigns in June 2018, February 2019, and May 2019

NOM-127	Ca^{2+} LNE	Mg^{2+} LNE	Na^{+} 200	K^{+} LNE	HCO_3^{-} 800	SO_4^{2-} 400	Cl^{-} 250	NO_3^{-} 44.30	% error	Facies
First sampling (June 2019)										
PCU-1	219.0	40.0	169.0	2.7	175.7	**462.5**	**271.6**	29.66	2.3	Ca–Cl
PCU-2	199.0	32.1	125.0	3.2	277.3	**403.2**	103.7	37.95	4.6	Ca-HCO_3
PCU-3	171.0	35.0	74.0	1.2	170.9	162.5	230.3	32.76	5.2	Ca-SO_4
PCU-4	120.0	26.0	24.0	1.0	135.3	143.7	128.0	30.54	− 0.7	Ca- HCO_3
PCU-5	126.0	28.0	24.0	1.2	177.0	120.0	124.8	18.60	2.3	Ca-SO_4
PCU-6	158.0	34.0	44.0	1.4	179.4	144.0	182.6	25.23	4.7	Ca-HCO_3
PCU-7	149.0	26.3	24.0	1.5	166.0	90.0	175.5	19.03	4.0	Ca-HCO_3
Second sampling (February 2019)										
PCU-1	200.0	33.0	118.0	5.1	258.3	**460.0**	105.4	36.30	1.6	Ca-HCO_3
PCU-2	ND	ND	ND	ND	ND	ND	ND	ND	ND	ND
PCU-3	129.0	25.7	28.3	1.4	266.7	167.5	37.4	30.98	2.1	Ca-SO_4
PCU-4	135.0	25.7	28.5	1.6	271.9	142.5	43.0	32.20	5.1	Ca-SO_4
PCU-5	123.0	25.0	25.0	1.0	158.0	132.0	122.4	25.60	0.6	Ca-HCO_3
PCU-6	145.0	28.0	39.9	1.5	284.5	187.5	51.8	32.75	3.5	Ca-SO_4
PCU-7	200.1	23.2	25.1	2.0	233.1	107.5	138.7	33.64	− 4.6	Ca- HCO_3-SO_4
Third sampling (May 2019)										
PCU-1	210.0	33.2	118.0	4.0	183.0	**457.2**	174.6	37.69	1.1	Ca- Cl
PCU-2	217.0	37.6	135.0	4.7	292.4	**421.7**	123.6	38.90	5.9	Ca-Na-SO_4-HCO_3
PCU-3	164.0	28.5	63.0	2.2	167.0	159.3	**293.2**	39.10	− 5.8	Ca–Cl-SO_4
PCU-4	150.0	26.6	39.3	1.6	154.0	131.0	177.2	35.46	2.7	Ca-HCO_3
PCU-5	136.0	24.0	26.3	2.0	162.0	143.0	116.5	30.20	2.8	Ca-HCO_3
PCU-6	151.0	26.1	31.6	1.8	176.0	169.0	190.7	33.70	− 5.2	Ca-HCO_3
PCU-7	138.0	34.0	28.0	1.7	159.0	112.0	172.3	31.30	3.0	Ca-SO_4

Values in bold exceed maximum permissible level MPL

ND No Data; *LNE* Limit Not Established.

Chevotareb's sequence may explain the presence of these types of water. This sequence can explain that Ca–HCO_3–SO_4 and Ca–SO_4–HCO_3 water may be related with an intermediate flow system and longer residence times. It is also important to consider infiltration of wastewater from sewer systems, which can cause groundwater to have high chloride and sulfate contents.

The water groups identified are consistent with Mora et al. (2017), who proposed that Ca–HCO_3 waters circulate through shale and limestone, while waters with Ca^{2+}, HCO_3^{-}, and SO_4^{2-} can be found in the Monterrey Valley. In this sense, the location of the study area and the hydrochemical data suggest that the groundwater is characteristic of a transition and discharge area, which is typical of the northeast portion of Monterrey Valley, where circulating water mixes with wastewater leaks from the sewer system and inverse cation exchange processes could occur (Torres-Martínez et al. 2020).

Heavy metals

The presence of heavy metals was analyzed based on water samples taken in February and May 2019 samplings. Of a total of 18 metals that were evaluated (Table 7), only Fe and Al concentrations were notable. The presence of Fe, Al, and Mn is usually caused by the dissolution of minerals. However, Fe and Mn are also commonly associated with the manufacture of iron and steel alloys (Navas and Batista 2003; Hernandez et al. 2017).

Groundwater quality

Potable water quality was determined by evaluating the results and comparing them with the national standards (NOM-127). This analysis shows that some of the parameters may pose a pollution problem, including Cl^{-}, SO_4^{2-}, Fe, Al, and total and fecal coliforms (Tables 6, 7, and 8).

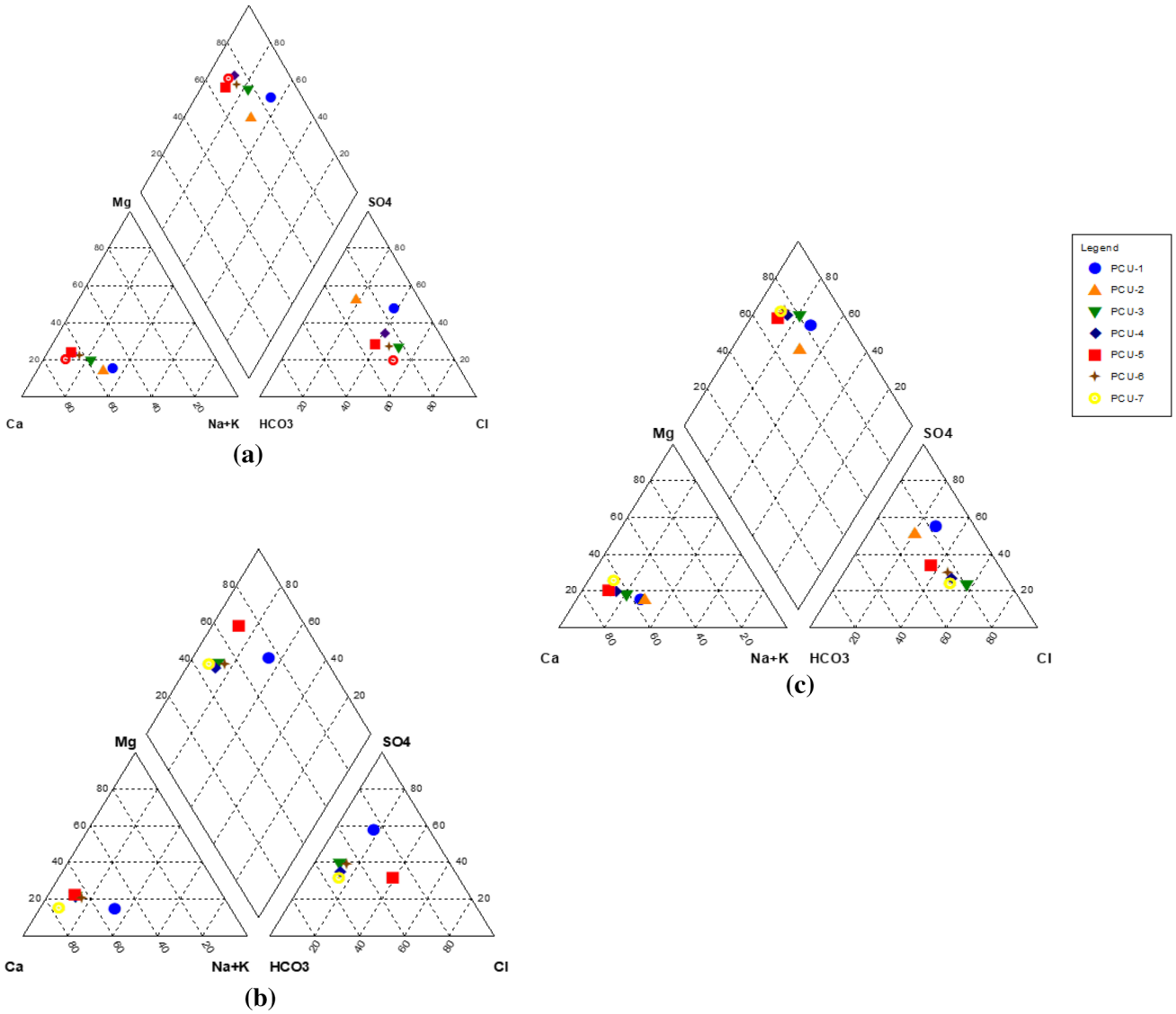

Fig. 7 Piper diagrams based on hydrochemical data from the study area: **a** June 2018, **b** February 2019, and **c** May 2019

Cl^- and SO_4^{2-} concentrations in the June 2018 and May 2019 samplings were very similar. In both samplings, the highest concentrations of these ions occurred in PCU-1 and PCU-2 and exceeded the maximum limit stipulated by NOM-127 (Cl^- 250 mg/L and SO_4^{2-} 400 mg/L). PCU-2 was also over this limit, but only for SO_4^{2-} concentrations. In June 2018, the Cl^- and SO_4^{2-} concentrations in PCU-1 were 462.5 and 271.6 mg/L, respectively, and in the well PCU-2 the SO_4^{2-} concentrations was 403.2 mg/L. In May 2019, only the SO_4^{2-} concentrations in PCU-1 and PCU-2 were over this limit with values of 457.2 and 421.7 mg/L, respectively. It is important to mention that the Cl^- concentration in PCU-3 was 293.2 mg/L which is over the maximum limit stipulated by NOM-127 (Table 6).

With regard to NO_3^- concentrations (Table 6), the highest values were found in the May 2019 samplings from PCU-1, PCU-2, and PCU-3 (37.69, 38.90 and 39.10 mg/L, respectively), however, none of the samples exceeded the maximum permissible level (MPL) established by NOM-127 (NO_3^-: 44.30 mg/L).

While Cl^-, and SO_4^{2-} ions naturally exist in groundwater, and considerable quantities are present in arid zones, these ions can also be attributed to the infiltration of wastewater and/or the use of treated wastewater to irrigate the UANL-university's green areas. Another likely cause of these concentrations is the use of water from the lagoon in Niños Héroes Park to irrigate green areas. This lagoon has no circulation, and the water is mixed with the park's wastewater.

Table 7 Heavy metal concentrations for sampling campaigns in February 2019 and May 2019

PARAMETER	PCU-1	PCU-2	PCU-3	PCU-4	PCU-5	PCU-6	PCU-7	NOM-127
Second sampling (February 2019)								
Al	0.008	ND	0.004	0.005	0.006	0.005	0.008	0.2
As	0.0004	ND	0.0005	0.0005	0.0004	0.0004	0.0006	0.025
Ba	0.032	ND	0.042	0.049	0.111	0.062	0.120	0.7
Br	0.0004	ND	0.0003	0.0002	0.0001	ND	0.0001	LNE
Cd	0.0003	ND	0.0001	0.0002	0.0001	0.0001	0.0002	0.005
Cr	0.001	ND	0.002	0.003	0.004	0.005	0.006	LNE
Cu	0.002	ND	0.001	0.001	0.001	0.002	0.002	2.0
Fe	**0.02**	**ND**	**0.03**	**0.04**	**0.05**	**0.06**	**0.06**	**0.3**
Hg	0.0004	ND	0.0005	0.0006	0.0007	0.0008	0.0009	0.001
Mn	**0.007**	**ND**	**0.004**	**0.002**	**0.001**	**0.003**	**0.015**	**0.15**
Mo	0.001	ND	0.001	0.001	0.002	0.001	0.001	LNE
Ni	0.001	ND	0.001	0.001	0.001	0.001	0.001	LNE
Pb	0.00008	ND	0.00002	0.00003	0.00004	0.00005	0.00006	0.01
Sb	0.0002	ND	0.0001	0.0001	0.0001	0.100	0.0003	LNE
Se	0.002	ND	0.002	0.003	0.002	0.003	0.003	LNE
Tl	0.0002	ND	0.0003	0.0004	0.0005	0.0006	0.0002	LNE
U	0.002	ND	0.006	0.002	0.002	0.002	0.002	LNE
Zn	0.016	ND	0.011	0.005	0.008	0.019	0.019	5.0
Third sampling (May 2019)								
Al	**0.005**	**0.036**	**0.006**	**0.18**	**0.006**	**0.0103**	**0.091**	**0.2**
As	0.001	0.001	0.001	0.001	0.001	0.001	0.001	0.025
Ba	0.032	0.065	0.029	0.040	0.210	0.051	0.107	0.7
Br	0.0001	0.0001	0.0001	0.0001	0.0001	0.0001	0.0001	LNE
Cd	0.00006	0.00015	0.00001	0.00001	0.00001	0.00012	0.00024	0.005
Cr	0.001	0.001	0.001	0.003	0.003	0.001	0.002	LNE
Cu	0.006	0.002	0.001	0.001	0.001	0.001	0.002	2.0
Fe	**0.1**	**0.13**	**0.02**	**0.85**	**0.1**	**0.29**	**0.29**	**0.3**
Hg	0.0002	0.0002	0.0002	0.0002	0.0002	0.0002	0.0002	0.001
Mn	**0.003**	**0.004**	**0.001**	**0.063**	**0.003**	**0.024**	**0.018**	**0.15**
Mo	0.0014	0.0013	0.0014	0.002	0.0013	0.0014	0.0017	LNE
Ni	0.020	0.001	0.0005	0.001	0.001	0.001	0.001	LNE
Pb	0.0025	0.0022	0.0002	0.0003	0.0002	0.0011	0.0010	0.01
Sb	0.0001	0.0002	0.0001	0.0001	0.0001	0.0003	0.0004	LNE
Se	0.0041	0.0035	0.0036	0.0039	0.0025	0.0035	0.0034	LNE
Tl	0.0001	0.0001	0.0002	0.0001	0.0006	0.0001	0.0001	LNE
U	0.0024	0.0023	0.0024	0.0020	0.0019	0.0022	0.0019	LNE
Zn	0.0686	0.008	0.0327	0.0239	0.0091	0.0159	0.0204	5

Values in bold exceed maximum permissible level MPL

ND no data; *LNE* Limit Not Established)

These same factors may also be related to the presence of high NO_3^- concentrations. Some authors have considered these ions to be indicators of possible contamination (Custodio and Llamas 1983; Werner 1996; Sawyer et al. 2001; Jayaprakash et al. 2008).

Regarding Fe and Al concentrations, these were close to the MPL only in the May 2019 sampling, particularly in PCU-4 (0.85 and 0.18 mg/L, respectively), which had the highest concentrations of these heavy metals. Their possible sources include corrosion of the equipment installed in the well and its lack of maintenance, as well as the TERNIUM steel company located to the east of the study area. However, the steel industry is very likely to be the main reason for the Fe and Al found, and although this situation does not represent a serious groundwater pollution problem, the Fe concentration does exceed the MPL and the Al concentration is

Table 8 Total and fecal coliform analysis for sampling campaigns in February 2019 and May 2019

Parameter	Well	Second Sampling (February 2019)	Third Sampling (May 2019)
Total coliforms (MPN/100 mL)	PCU-1	< 2	< 2
	PCU-2	ND	< 2
	PCU-3	< 2	< 2
	PCU-4	15	23
	PCU-5	7	13
	PCU-6	1	5
	PCU-7	2	8
Fecal coliforms (MPN/100 mL)	PCU-1	< 2	< 2
	PCU-2	ND	< 2
	PCU-3	< 2	< 2
	PCU-4	< 2	< 2
	PCU-5	< 2	< 2
	PCU-6	< 2	< 2
	PCU-7	< 2	< 2

Values in MPN (most probable number)/100 mL)

ND No data.

very close to it. Bacteriological analyses are very important to potability given that coliforms can cause many infectious diseases (Villarreal et al. 2013), since their main source is wastewater (Lizárraga 2003).

According to Mexican standard NOM 127, the MPL for total and fecal coliforms is the absence of the bacteria or levels below the limit of detection. However, the analysis of the samples collected in February and May 2019 confirm the presence of total and fecal coliforms (Table 8). In February 2019, total coliforms ranged from < 2 to 15 MPN/100 mL and fecal coliform was under < 2 MPN/00 mL. In May 2019, the total coliform range increased significantly, from < 2 to 23 MPN / 100 mL, while fecal coliform remained the same (< 2 MPN /100 mL). It should be noted that bacteriological organisms were found in PCU-4, PCU-5, PCU-6, and PCU-7 (Table 8), which are located in areas where leaks from the sewer system have been identified.

Groundwater vulnerability

Depth of groundwater (*D*)

Depth of groundwater determines the depth to which a contaminant would have to travel before it reaches the water table (Al-Zabet 2002). Depth data were taken from measurements carried out in the ten study wells during May 2019. A depth of groundwater map was created in ArcGIS and converted to raster format (Fig. 8a).

The depth of the groundwater ranged from 11 to 16 m below ground table level, which corresponds to classifications 3 and 5 on the scale proposed by Aller et al. (1987) (Fig. 8a).

Net recharge (*R*)

Rainfall is an important factor in groundwater vulnerability. The intensity of precipitation affects the contaminant's movement, its infiltration, and whether it reaches the saturated layer. Net recharge ranged from 60 to 62 mm, which corresponds to classification 3 on the scale proposed by Aller et al. (1987) (Fig. 8b).

Aquifer media (*A*)

This parameter represents the geological formation of the upper layer of the aquifer, and according to the permeability of the materials, a rating is assigned to each of them (Gupta 2014). This map was prepared from stratigraphic profiles (Table 4). The aquifer media are mostly sand, gravel, and medium-cemented gravel, with clay silt, sand, and gravel in the vadose zone. According to the classification by Aller et al. (1987), ratings of 6 and 4 were assigned, respectively (Fig. 8c).

Soil media (*S*)

The main land use in the study area is urban. The soil media represent the topsoil layer, which extends to the weathered zone a few meters down from the surface. This significantly impacts the amount of recharge water that infiltrates deeper into the aquifer, thereby affecting the downward movement of contaminants into the vadose zone (Lee 2003). To differentiate between the impact of the vadose zone and the aquifer media, a soil depth of less than ~ 2 m to the groundwater table was considered. Just over 50% of the area contained silty clay soil with gravel. A rating of 9 was assigned to clay, gravel, and sand and 7 to silty clay (Fig. 8d).

Topography or slope (*T*)

The topography refers to the slope of the terrain surface. Slope influences the contact time between water and soil, and therefore, the degree of infiltration. Steeper slopes have less infiltration (and less vulnerability), while water remains for a longer period of time on shallow slopes, allowing more water to infiltrate (and increasing vulnerability). According to a 30 cm resolution Lidar image, the study area has a slight slope (0.0004–0.28) corresponding to a rating of 10 on the scale proposed by Aller et al. (1987) (Fig. 9a).

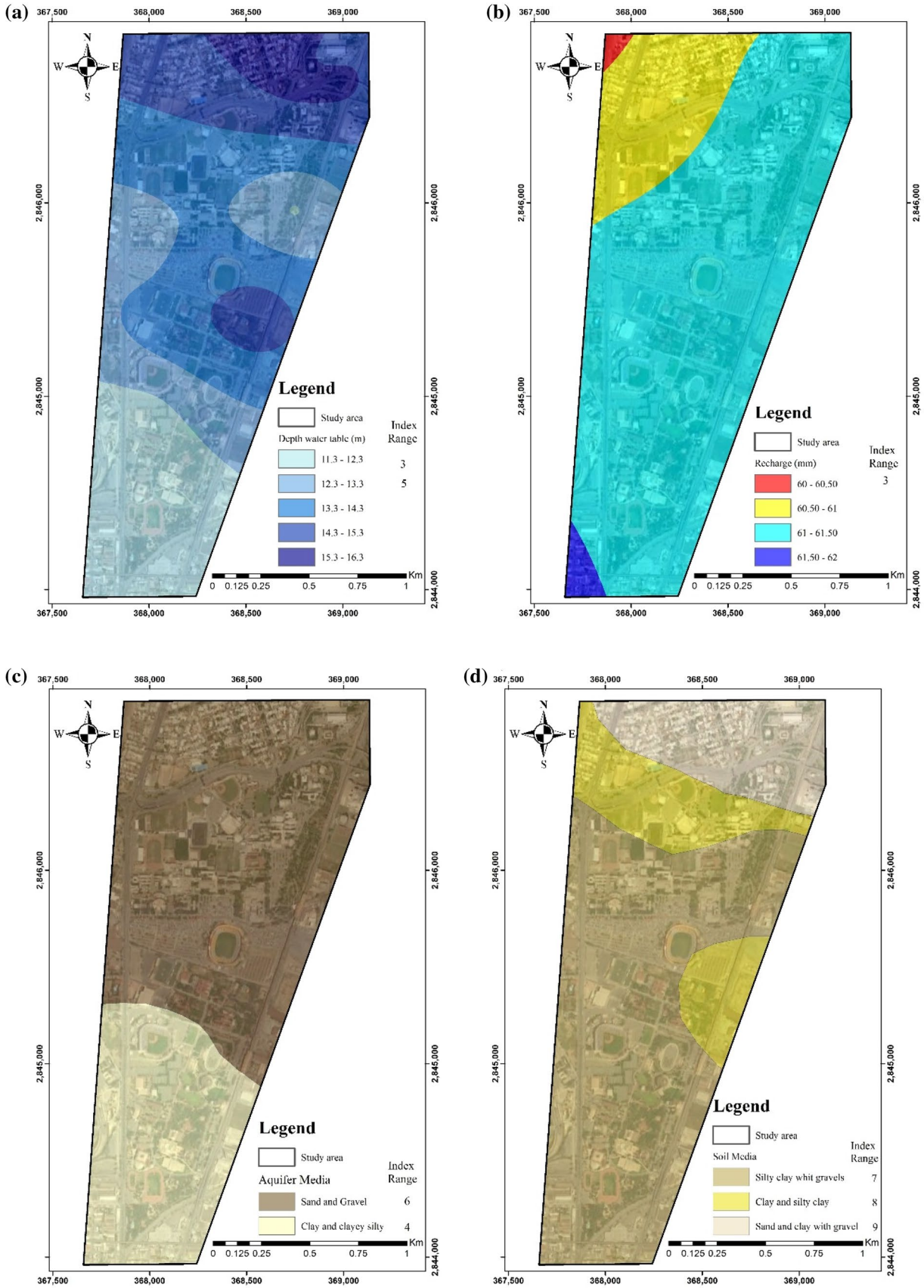

Fig. 8 **a** Depth of groundwater, **b** Net recharge, **c** Aquifer media, **d** Soil media

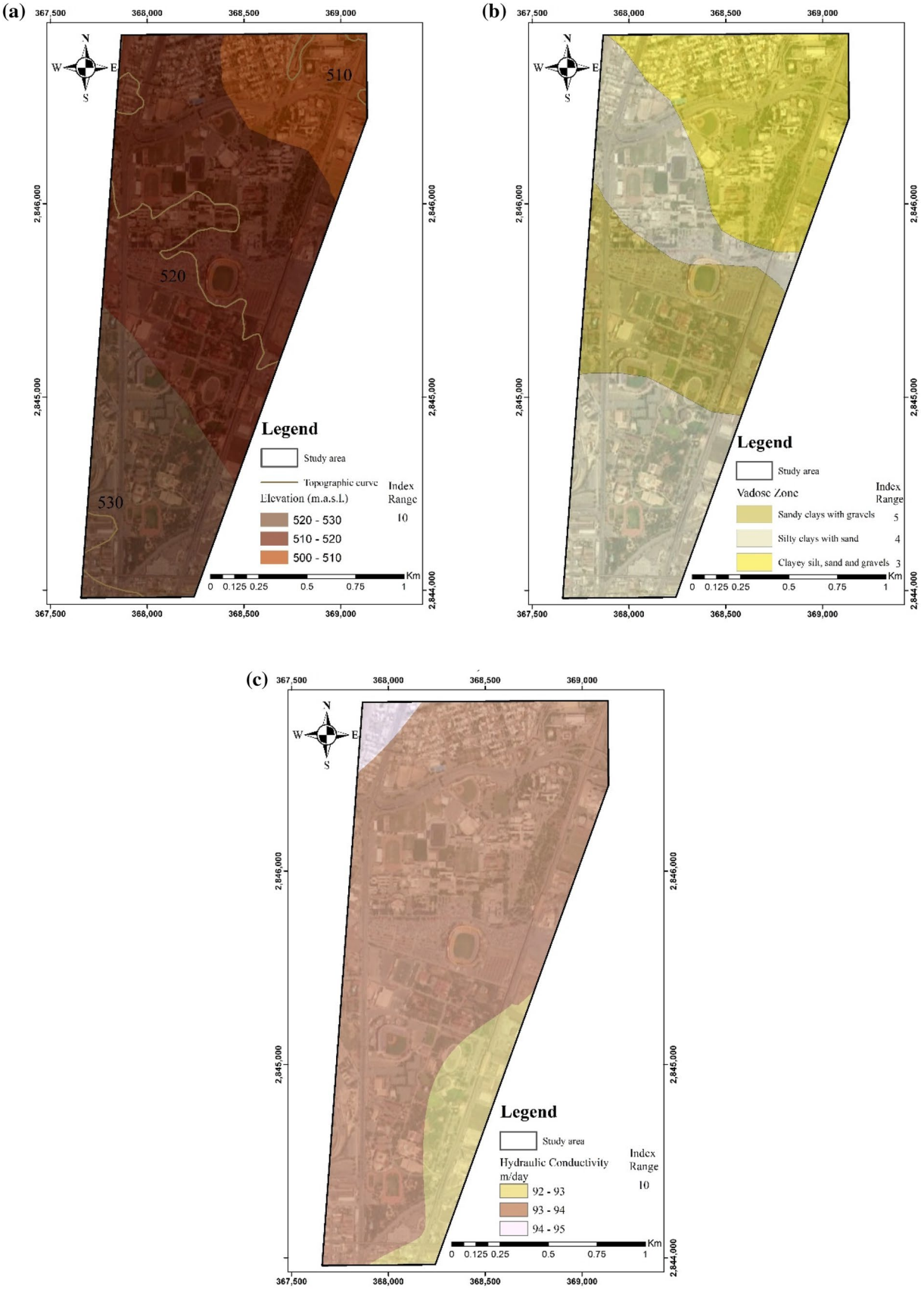

Fig. 9 **a** Topography, **b** Vadose zone, **c** Hydraulic conductivity

Vadose zone (*I*)

The information about this parameter was obtained from stratigraphic profiles. The vadose zone in the study area consists of i) clayey silt, sand, and loose grave, ii) calcium clay, silty clay, and sand, and iii) sandy clay with gravel. The units containing clay are less vulnerable, while those with gravel and sand are more vulnerable. They were assigned ratings of 5 and 3, according to their properties (Fig. 9b).

Hydraulic conductivity of the aquifer (*C*)

Hydraulic conductivity is an important parameter of an aquifer, which is a characteristic of its geological properties. Since it governs the rate at which water flows through the aquifer's saturated zone, this parameter determines contaminant transport. According to Hernández (1999), hydraulic conductivity ranges from 90 to 95 m/day (average = 93 m/day), which corresponds to a rating of 10 on the scale proposed by Aller et al. (1987) (Fig. 9c).

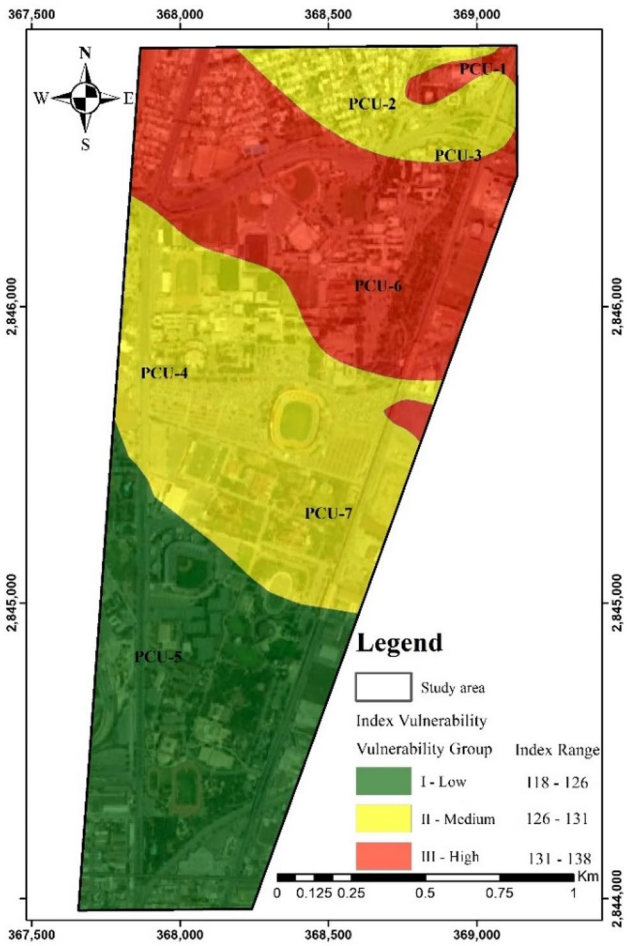

Fig. 10 Vulnerability index map of the study area

The DRASTIC method was used to produce the map shown in Fig. 10. As can be seen, vulnerability was found to be low in roughly 60% of the area, and medium and high in around 20% of the area, each. Low vulnerability was identified in the southern portion of the study area, and medium and high vulnerability to groundwater contamination was found in the rest of the study area.

It is important to highlight that the areas with medium and high vulnerability are areas requiring attention in order to prevent vulnerability from increasing as the leaching of pollutants increases. Therefore, it is important to implement measures to reduce contamination from anthropogenic activities.

The maps in Fig. 11 show how the different water quality parameters analyzed relate with the vulnerability of the study area. Electrical conductivity, SO_4^{2-}, NO_3^-, Fe, Al, and total coliforms were integrated into the vulnerability index map. As shown, groundwater contamination in areas with medium and high vulnerability is related with the concentrations of all the parameters studied (electrical conductivity, SO_4^{-2}, NO_3^-, Fe, Al, and total coliforms).

The map also shows low vulnerability in the southern portion of the study area. However, this condition does not eliminate the risk that groundwater contamination problems could arise in these areas since the sources of contamination that were identified have not been eliminated. Furthermore, as in the rest of the study area, leaks or fissures in the sewer system may exist, as indicated by the high concentrations of sulfates and total coliforms found in well PCU-5 (Tables 5 and 7). In particular, the sewer system belonging to a hospital and two sports stadiums should be considered. Roughly, 50,000 people typically gather in the stadiums every weekend. It is also important to consider the lagoon in Niños Héroes Park as another possible factor that can influence coliform values, since this lagoon serves as part of the drainage of the park and this water is extracted to irrigate green areas.

A method to validate the DRASTIC model was performed based on the Cl^-, SO_4^{2-}, and NO_3^- concentrations in the groundwater (Fig. 12). While the presence of Cl^- and SO_4^{2-} in groundwater is related with anthropogenic activities, NO_3^- is the indicator that is most used to identify the anthropic impact on groundwater (Freeze and Cherry 1979; Martinez et al. 2014; Zendehbad 2019). It is important to mention that the distribution and concentration of these indicators depend on various factors, such as soil dynamics, the recharge rate, the movement of groundwater, and the soil contamination load (Ahmed et al. 2015). The graph in Fig. 12 presents the average Cl^-, SO_4^{2-}, and NO_3^- concentrations for the different classes of vulnerability. PCU-5 is located in the low vulnerability zone, PCU-3, PCU-4, and PCU-7 are in the medium vulnerability zone, and PCU-1, PCU-2, and PCU-6 are in the high vulnerability zone.

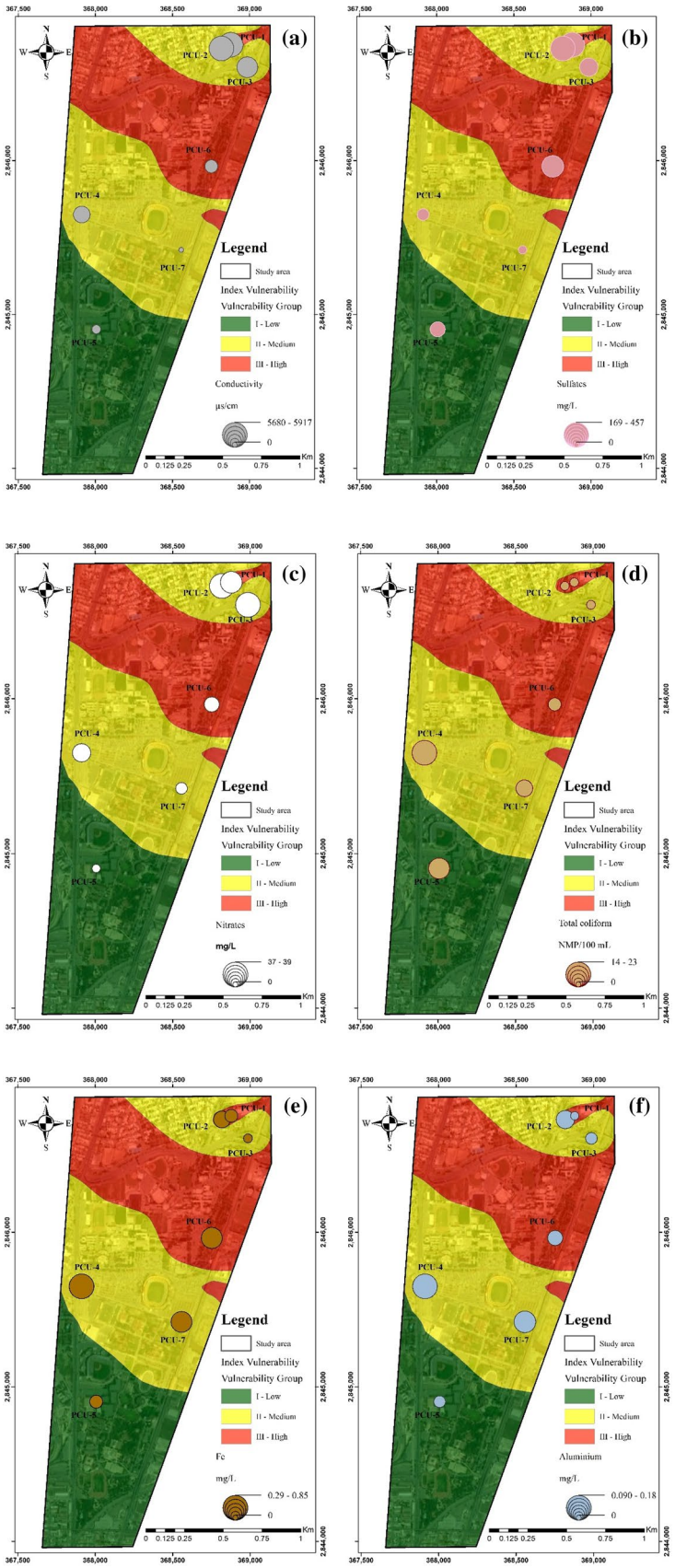

Fig. 11 **a** Spatial distribution of electrical conductivity; **b** SO_4^{-2}; **c** NO_3^{-}; **d** total coliforms; **e** Fe, and **f** Al, integrated into the vulnerability index map

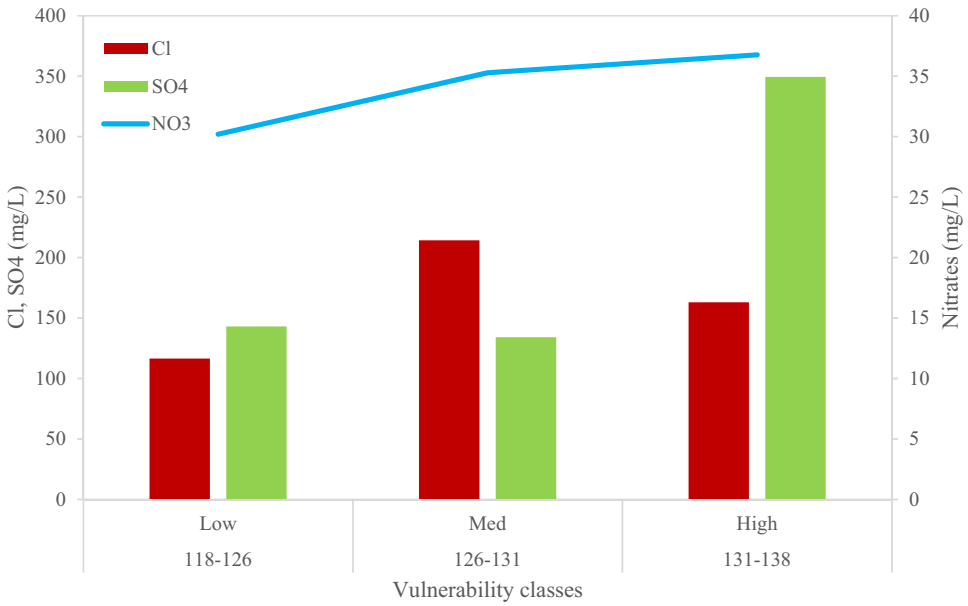

Fig. 12 Validation of the DRASTIC model by comparing average Cl^-, SO_4^{2-}, and NO_3^- concentrations for different vulnerability classes

Cl^- concentrations (214 mg/L) significantly increased from the low to medium vulnerability zones, while average SO_4^{-2} remained the same (134 mg/L). From the medium to the high vulnerability zones, average Cl^- concentrations decreased and average SO_4^{-2} concentrations increased significantly. In the case of NO_3^- concentrations, these increased as vulnerability increased, highlighting the increase that occurs from the low to medium vulnerability zone. The increased concentrations in the high vulnerability zone can be explained by the evidence of leaks from the sewer system in that area, and as explained in previous paragraphs, groundwater mixes with leaks from the sewer system in the northern and northeast portion of the Monterrey Valley.

Conclusions

In general, groundwater levels did not change significantly, and ranged from 498 to 520 m.a.s.l. The groundwater was found to flow from southwest to northeast. The most significant hydrodynamic changes occurred in the years 2016 and 2017, when the groundwater flow changed mainly due to exploitation. It is important to mention that the groundwater table was very stable even though water was extracted from the wells to meet various needs.

Based on the physicochemical parameters and the groundwater quality analysis, electrical conductivity, SO_4^{2-}, Cl^-, Fe, Al, and coliform concentrations indicate that the groundwater may be contaminated by leaks in the sewer system and the resulting infiltration of those waters. The heavy metal concentrations that were identified may be due to activities by the TERNIUM company, a steel company located very close to the study area. However, this needs to be verified by monitoring the wells on the company's property, which this research work could not access due to several industry restrictions.

The vulnerability map made it possible to view zones with different degrees of vulnerability. The DRASTIC model was validated using Cl^-, SO_4^{2-}, and NO_3^- as indicators of human interaction with the groundwater environment. Greater concentrations of these indicators were found primarily in the high vulnerability zone, which can be explained by leaks from the sewer system.

In this sense, it is pertinent that a specific study of groundwater contamination be carried out due to the leaks from the sewage system to know the direct influence on the quality of the groundwater in the different uses.

In addition to the above, it is necessary to take the necessary managements with the authorities and the corresponding companies to have access to the different private wells and thus be able to make an inventory of the wells that are currently in operation, which together with the potential sources of contamination, can be considered in a water quality monitoring network.

In the same way, as mentioned by other studies, to use vulnerability maps for implementing and prioritizing policies on aquifer protection and water resources management can be a very useful tool.

Authors' contributions Optional.

Funding Not applicable.

Data availability The data used to support the findings of this study are available from the corresponding author upon request.

Declarations

Conflict of interest The authors declare that they have no conflict of interest.

References

Ahmed I, Nazzal Y, Zaidi FK, Al-Arifi SN, Ghrefat H, Naeem M (2015) Hydrogeological vulnerability and pollution risk mapping of the Saq and overlying aquifers using the DRASTIC model and GIS techniques, NW Saudi Arabia. Environ Earth Sci. https://doi.org/10.1007/s12665-015-4120-5

Aller L, Lehr JH, Petty R, Bennett T (1987) DRASTIC: A Standardized system to evaluate groundwater pollution potential using hydrogeologic settings. National Water Well Association, Worthington, Ohio, United States of America, pp 1–163

AlSuhaimi AO, AlMohaimidi KM, Momani KA (2017) Preliminary assessment for physicochemical quality parameters of groundwater in Oqdus Area, Saudi Arabia. J Saudi Soc Agric Sci 18(1):22–31. https://doi.org/10.1016/j.jssas.2016.12.002

Alva Niño E (1997) Estudio Geológico-Hidrogeológico de la región noroeste (Sierra las mitras- cerro el Topo- cerro el Durazno) de Monterrey, Estado de Nuevo León. Universidad Autónoma de Nuevo León (UANL), Facultad de Ciencias de la Tierra, Tesis, pp 1–118

Al-Zabet T (2002) Evaluation of aquifer vulnerability to contamination potential using the DRASTIC method. Environ Geol 43:203–208. https://doi.org/10.1007/s00254-002-0645-5

Asadi P, Ataie-Ashtiani B, Beheshti A (2017) Vulnerability assessment of urban groundwater resources to nitrate: the case study of Mashhad, Iran. Environ Earth Sci 76(41):1–15. https://doi.org/10.1007/s12665-016-6357-z

Instituto Nacioal de Geografia (INEGI) (2008). Características edafológicas, fisiográficas, climáticas e hidrográficas de México. p32.

Instituto Nacioal de Geografia (INEGI) (2020). Censos y Encuestas Intercensales. Series originales. Datos para Nuevo León. consultado el 3 de agosto de 2020.

Chenini I, Zghibi A, Kouzana L (2015) Hydrogeological investigations and groundwater vulnerability assessment and mapping for groundwater resource protection and management: State of the art and a case study. J Afr Earth Sci 109:11–26. https://doi.org/10.1016/j.jafrearsci.2015.05.008

Comision Nacional del Agua (CONAGUA). (2019). Estación Meteorológica de Monterrey.

Custodio E, Llamas MR (1983) Hidrología subterránea, vol 2. Editorial Omega, Barcelona, pp 1–2350

da Silva Peixoto F, Cavalcante IN, Gomes DF (2020) Influence of land use and sanitation issues on water quality of an urban aquifer. Water Resour Manage 34:653–674. https://doi.org/10.1007/s11269-019-02467-6

Daneshian H, Kalantari N, Alijani F (2020) Hydrochemistry and stable isotopes characteristics of groundwater in an urban aquifer southwest of Iran. Geopersia 8(1):1–18. https://doi.org/10.22059/geope.2020.294287.648520

Diaz Delgado C., Esteller Alberich, M. V., Lopez Vera F. (2006). Recursos Hídricos: Conceptos Bàsicos y Estudios de Caso en Iberoamerica. Red iberoamericana de Potabilización y Depuración del Agua, Centrp Interamericano del Recursos del Agua, Facultad de Ingenieria, Universidad Autónoma del Estado de México (México) y Piriguazú (Uruguay).

Dragon K, Gorski J (2015) Identification of groundwater chemistry origins in a regional aquifer system (Wielkopolska region, Poland). Environ Earth Sci 73:2153–2167. https://doi.org/10.1007/s12665-014-3567-0

Freeze A, Cherry J (1979) Groundwater Pollution. Prentice Hall, New Jersey U.S.A., p 598

Gárfias J, Llanos H, Franco R, Martel R (2017) Estimación de la vulnerabilidad del acuífero del valle de Toluca mediante la combinación de un método paramétrico y el transporte advectivo. Boletin Geologico y Minero. 128(1):28–42. https://doi.org/10.21701/bolgeomin.128.1.002

Gobierno del Estado de Nuevo Leon (2016). Plan Estatal de Desarollo 2016-2021. Nuevo Leon, Mexico. 257pp

González-Abraham N., (2011). Determinación de los sistemas de flujo del agua subterránea y caracterización de sus componentes en regiones desérticas: el caso de Loreto, Baja California Sur. Tesis Doctoral. Centro de investigaciones biológicas del noreste, S.C., p 110.

Guerra-Cobian VH, Ferrriño AL, Cavazos RA (2015) Simulacion hidrològica utilizando precipitacion asociada a eventos de tipo ciclònico: Caso de estudio cuenca del rìo La Silla. IV Jornadas de Ingenieria del Agua: La precipitacion y los procesos erosivos. Universidad de Cordoba, España, p 12

Gupta N (2014) Groundwater vulnerability assessment using DRASTIC method in Jabalpur district of Madhya Pradesh. Int J Recent Technol Eng (IJRTE) 31(3):36–43 (**ISSN: 2277-3878**)

Hassane AB, Leduc C, Favreau G, Bekins BA, Margueron T (2016) Impacts of a large Sahelian city on groundwater hydrodynamics and quality: example of Niamey (Niger). Hydrogeol J 24:407–423. https://doi.org/10.1007/s10040-015-1345-z

Hernández, L. (1999). Caracterización del acuífero de Ciudad Universitaria de la Universidad Autónoma de Nuevo León. Tesis de Maestría. Nuevo León, México. Facultad de Ingeniería Civil, Universidad Autónoma de Nuevo León. 59pp.

Hernandez Gonzalez, S., Gòmez Vega, A., Juarex Yañez, P., Hernandez Zàrate G. (2017). Determinaciòn de hierro y manganeso en el agua subterrànea del municipio de Apan, Hidalgo, Mèxico. Ciencia y tecnologìa universitaria, 5(1): 6pp. ISSN:2007–7750.

Hernández-Espriú A, Reyna-Gutiérrez JA, Sánchez-León E et al (2014) The DRASTIC-Sg model: an extension to the DRASTIC approach for mapping groundwater vulnerability in aquifers subject to differential land subsidence, with application to Mexico City. Hydrogeol J 22:1469–1485. https://doi.org/10.1007/s10040-014-1130-4

Huang G, Liu C, Sun J, Zhang M, Jing J, Li L (2018) A regional scale investigation on factors controlling the groundwater chemistry of various aquifers in a rapidly urbanized area: A case study of the Pearl River Delta. Sci Total Environ 625:510–518. https://doi.org/10.1016/j.scitotenv.2017.12.322

Hussain Y, Ullah SF, Hussain MB, Aslam AQ, Akhter G, Martinez-Carvajal H, Cárdenas-Soto M (2017) Modelling the vulnerability of groundwater to contamination in an unconfined alluvial aquifer in Pakistan. Environ Earth Sci. https://doi.org/10.1007/s12665-017-6391-5

Jayaprakash M, Giridharan L, Venugopal T, Kumar Krishna SP, Periakali P (2008) Characterization and evaluation of the factors affecting the geochemistry of groundwater in Neyveli, Tamil Nadu, India. Environ Geol 54:855–867. https://doi.org/10.1007/s00254-007-0868-6

Kazakis N, Voudouris KS (2015) Groundwater vulnerability and pollution risk assessment of porous aquifers to nitrate: Modifying the DRASTIC method using quantitative parameters. J Hydrol 525:13–25. https://doi.org/10.1016/j.jhydrol.2015.03.035

Lapworth DJ, Das P, Shaw A, Mukherjee A, Civil W, Petersen JO, Gooddya DC, Wakefieldd O, Finlaysone A, Krishanf G, Senguptab P, MacDonald AM (2018) Deep urban groundwater vulnerability in India revealed through the use of emerging organic contaminants and residence time tracers. Environ Pollut 240:938–940. https://doi.org/10.1016/j.envpol.2018.04.053

Lathamani R, Janardhana MR, Mahalingam B, Suresha S (2015) Evaluation of aquifer vulnerability using drastic model and GIS: a case study of Mysore City, Karnataka, India. Aquatic Procedia 4:1031–1038. https://doi.org/10.1016/j.aqpro.2015.02.130

Lee S (2003) Evaluation of waste disposal site using the DRASTIC system in southern Korea. Environ Geol 44:654–664

Li S, Ma S, Yu P, Li Y (2018a) Evaluation of groundwater vulnerability to contaminatión based on DRASTIC model and GIS in Tianjin plain area. IOP Conf Series Mater Sci Eng 301:1–6. https://doi.org/10.1088/1757-899X/301/1/2090

Li X, Wu H, Qian H, Gao Y (2018b) Groundwater chemistry regulated by hydrochemical processes and geological structures: A case study in Tongchuan, China. Water (Switzerland) 10(338):1–16. https://doi.org/10.3390/w10030338

Lizárraga Mendiola, L.G. (2003). Análisis y Evaluación del agua subterránea del área del tiradero municipal y la petaca, Linares, N.L., México. Tesis. UANL. 134pp

MacDonald AM, Bonsor HC, Ahmed KM, Burgess WG, Basharat M, Calow RC, Yadav SK (2016) Groundwater quality and depletion in the Indo-Gangetic Basin mapped from in situ observations. Nat Geosci 9(10):762–766. https://doi.org/10.1038/ngeo2791

Machiwal D, Jha MK, Singh VP, Mohan Ch (2018) Assessment and mapping of groundwater vulnerability to pollution: current status and challenges. Earth Sci Rev 185:901–927. https://doi.org/10.1016/j.earscirev.2018.08.009

Martín Del Campo MA, Esteller MV, Expósito JL, Hirata R (2014) Impacts of urbanization on groundwater hydrodynamics and hydrochemistry of the Toluca Valley aquifer (Mexico). Environ Monit Assess 186:2979–2999. https://doi.org/10.1007/s10661-013-3595-3

Martìnez D, Moschione E, Bocanegra E, Glok Galli M, Aravena R (2014) Distribution and origin of nitrate in groundwater in an urban and suburban aquifer in Mar del Plata, Argentina. Environ Earth Sci 72:1877–1886. https://doi.org/10.1007/s12665-014-3096-x

Mora A, Mahlknecht J, Rosales-Lagarde L et al (2017) Assessment of major ions and trace elements in groundwater supplied to the Monterrey metropolitan area, Nuevo León, Mexico. Environ Monit Assess 189(394):1–15. https://doi.org/10.1007/s10661-017-6096-y

Nanou E-A, Zagana E (2018) Groundwater Vulnerability to Pollution Map for Karst Aquifer Protection (Ziria Karst System, Southern Greece). Geosciences 8(125):1–15. https://doi.org/10.3390/geosciences8040125

Navarro-Solís et al (2016) Integrative methodology for the identification of groundwater flow patterns: application in a Semi-Arid region of México. Appl Ecol Environ Res 14(4):645–666

Navas Medina, E. & Batista Cabrera, A (2003). Utilizaciòn del mineral de Manganeso (pirolusita) en la produccion de aceros al carbono. Minería y Geología Nos. 3 (4): 73–78. ISSN 0258 5979.

Neshat A, Pradhan B, Dadras M (2014) Groundwater vulnerability assessment using an improved DRASTIC method in GIS. Resour Conserv Recycl 86:74–86. https://doi.org/10.1016/j.resconrec.2014.02.008

Ortega Gaucin D, Velasco D (2013) Impacto de las sequías en Nuevo León. Ciencia UANL 16(63):8–14

Ouedraogo I, Defourny P, Vancooster M (2016) Mapping the groundwater vulnerability for pollution at the pan African scale. Sci Total Environ 544:939–953. https://doi.org/10.1016/j.scitotenv.2015.11.135

Paredes, J.; Esteller, M.V., Expósito, J.L.. (2018). Determinación de la vulnerabilidad de la Contaminación del acuífero del Valle de Toluca mediante el método SINTACS. Ciencias del Agua: Perspectivas desde la academia. UAEMex. 53–66. ISBN: 978-607-422-910-3.

Pórcel R, Schüth C, León-Gómez H, Hoppe A, Lehné R (2014) Land-Use Impact and Nitrate Analysis to Validate DRASTIC Vulnerability Maps Using a GIS Platform of Pablillo River Basin, Linares, N.L., Mexico. Int J Geosci 5:1468–1489. https://doi.org/10.4236/ijg.2014.512120

Servicios de Agua y D renage de Monterrey (SAyDM) (2018). Reporte Tecnico Acuifero Campo de Pozos Monterrey.

NOM-230-SSA1–2002. Salud ambiental. Agua para uso y consumo humano, requisitos sanitarios que se deben cumplir en los sistemas de abastecimiento públicos y privados durante el manejo del agua. Procedimientos sanitarios para el muestreo.

NOM-127-SSA1-1994 (2000). Salud ambiental. Agua para uso y consumo humano. Límites permisibles de calidad y tratamientos a que debe someterse el agua para su potabilización. Diario Oficial de la Federación, 20 de junio de 2000.

Samantara MK, Padhi RK, Sowmya M, Kumaran P, Satpathy KK (2017) Heavy metal contamination, major ion chemistry and appraisal of the groundwater status in coastal aquifer, Kalpakkam, Tamil Nadu, India. Groundwater Sustain Dev 5:49–58. https://doi.org/10.1016/j.gsd.2017.04.001

Sawyer CN, McCarty PL, Parkin GF, de García A, Quigua DAA (2001) Química para ingeniería ambiental. McGraw-Hill, Bogotá, Colombia, p 685

Schirmer M, Leschik S, Musolff A (2013) Current research in urban hydrogeology—A review. Adv Water Resour 51:280–291. https://doi.org/10.1016/j.advwatres.2012.06.015

Shrestha S, John Semkuyu D, Pandey VP, Barcelo D (2016) Assessment of groundwater vulnerability and risk to pollution in Kathmandu Valley, Nepal. Sci Total Environ 556:23–35. https://doi.org/10.1016/j.scitotenv.2016.03.021

Silva González J.L., Francisco H., Jorge G. (2015). Estudio de microcuencas hidrológicas urbanas y perfiles hidroestratigráficos en la zona del campus "ciudad universitaria-uanl" aplicando técnicas de geomática. Tesis de licenciatura. p 157

Srinivasamoorthy K, Gopinath M, Chidambaram S, Vasanthavigar M, Sarma VS (2014) Hydrochemical characterization and quality appraisal of groundwater from Pungar sub basin, Tamilnadu, India. J King Saud Univ Sci 26:37–52. https://doi.org/10.1016/j.jksus.2013.08.001

Torres-Martínez JA, Mora A, Knappett PSK, Ornelas-Soto N, Mahlknecht J (2020) Tracking nitrate and sulfate sources in groundwater of an urbanized valley using a multi-tracer approach combined with a Bayesian isotope mixing model. Water Res 182:1–16. https://doi.org/10.1016/j.watres.2020.115962

Valcarce Ortega RM, Jiménez Reyes R (2016) Vulnerabilidad y riesgo de contaminación de la Cuenca Dolores-Sagua la Chica. Cuba Ingeniería Hidráulica y Ambiental 37(1):03–14

Villarreal-Treviño L, Vela M, Galán J (2013) Manual de prácticas de microbiología general. Primera edición. UANL. p 63

Waguespack J (2019). Characterization of a shallow urban aquifer in Atlanta, Georgia. Georgia State University, Thesis. https://scholarworks.gsu.edu/geosciences_theses/129. Accessed July 2020

Werner J (1996) Introducción a la Hidrogeología. Primera edición. Universidad Autónoma de Nuevo León, Linares, NL, p 174

Zendehbad SM, Cepuder P, Loiskandl W, Stumpp C (2019) Source Identification of nitrate contaminatiòn in the urban aquifer of Mashhad, Iran. J Hydrol Reg Stud 25(100618):1–14. https://doi.org/10.1016/j.ejrh.2019.100618